SPECIAL ISSUE - RESEARCH ARTICLE

Journal of
RAMAN
SPECTROSCOPY WILEY

Raman spectroscopy potentiality in the study of geopolymers reaction degree

Maria Cristina Caggiani[1] | **Alessia Coccato[1]** | **Germana Barone[1]** |
Claudio Finocchiaro[1] | **Maura Fugazzotto[1,2]** | **Gabriele Lanzafame[1]** |
Roberta Occhipinti[1] | **Antonio Stroscio[1]** | **Paolo Mazzoleni[1]**

[1]Department of Biological, Geological and Environmental Sciences, University of Catania, Catania, Italy

[2]Department of Humanities, University of Catania, Catania, Italy

Correspondence
Germana Barone, Department of Biological, Geological and Environmental Sciences, University of Catania, Catania, Italy.
Email: gbarone@unict.it

Abstract

Alkali-activated materials (AAMs) and "geopolymers" are inorganic polymeric materials obtained by mixing of solid aluminosilicate precursors with an alkaline solution (generally, KOH or NaOH and Na_2SiO_3 mixed in various ratios). This class of aluminosilicate materials has emerged as a greener alternative to traditional concrete, for large-scale as well as for niche applications such as conservation and restoration of built heritage. In this work we apply Raman spectroscopy both to aluminosilicate precursors (metakaolin, pumice, volcanic ash, volcanic soils, clayey sediments, ceramic waste) and to the respective AAMs. In the field of vibrational spectroscopy, Raman is much less employed in the literature with respect to Fourier transform infrared (FTIR) to have insights into the alkali activation process from a molecular point of view. The aim of this paper is to investigate the potentiality of a Raman approach to the comparison of the employed raw materials with the respective AAMs. Raman analyses during the first hours of geopolymerization were also carried out on the clayey sediments and ceramic waste-based products. The results, differentiated according to the employed precursors, exhibit spectra relative to crystalline and amorphous phases that can give an indication about the newly formed aluminosilicate gel.

KEYWORDS
alkali-activated materials, aluminosilicates, amorphous phases, geopolymerization

1 | INTRODUCTION

Alkali-activated materials (AAMs), including those classified as geopolymers,[1] have been intensively studied and promoted in the last decades as low-carbon binder alternatives to Portland-based cements, in response to growing global concerns over CO_2 emissions from the construction sector.[2–9] AAMs can be generated from a variety of industrial minerals such as kaolinite and feldspars and from industrial solid residues or wastes such as fly ashes, metallurgical slags, and mine wastes.[2,6,10] Thus, their versatility and local adaptability make them a

powerful tool in the development of worldwide sustainable construction industry. In the framework of the Italian National Research Program "Advanced Green Materials for Cultural Heritage," local Sicilian raw materials and industrial wastes are being used as precursors for geopolymers production with the aim to contribute at reducing the carbon footprint and the environmental impact of building materials industrial production.

AAMs are produced from a mixture of several aluminosilicate materials (with high contents of Si and Al) along with an alkaline-activating solution of hydroxides (Na^+, K^+, or Ca^+) and silicates (Na^+ and K^+) and even carbonates or sulfates.[2] The result is a hardened binder based on a combination of hydrous alkali-aluminosilicate and/or alkali-alkali earth-aluminosilicate phases. Based on the nature of their cementitious components, alkaline materials may be classified as high-calcium and low-calcium cements. In the first model, Ca- and Si-rich materials are the main components, and the reaction product is a calcium aluminosilicate hydrate (C-A-S-H) gel, which takes Al in its structure, similar to the gel obtained during Portland cement hydration.[11] In the second system, the materials activated comprise primarily Al and Si. The main reaction product is a 3D inorganic alkaline polymer, a sodium aluminosilicate hydrate (N-A-S-H) gel with a highly cross-linked, disordered pseudo-zeolitic structure.[8,9,12,13] This gel is also called geopolymer or inorganic polymer. The negative charge related to the substitution of Si^{4+} by Al^{3+} is balanced by alkali-metal cations in the gel framework. In the present study, we focused on the latter system.

Several parameters must be analyzed selecting the raw materials to produce geopolymers, such as the reactive (amorphous) silica content and particle size.[14]

The reactivity of raw materials depends on their Al_2O_3 and SiO_2 content. Moreover, the alteration of Si/Al molar ratio allows the synthesis of materials with different structures as the aluminum atoms cross-link chains of SiO_4 and $MAlO_4$ tetrahedra (where M is a monovalent cation, typically Na^+ or K^+). The polymer formation rate is also influenced by the type of the alkaline metal and by the concentration of the activating solution on the development of the microstructure of the gel framework.

At the end of the reaction process, several phases are present in the system. These include unreacted particles, partially reacted particles, newly formed (alumino)-silicate gel, smaller (alumino)-silicate species liberated from the network, dissolved alkali-metal hydroxides, and water.[15,16]

The spectroscopic techniques generally used to evaluate the structure of the AAMs at short-range length scale include Fourier transform infrared (FTIR) and nuclear magnetic resonance (NMR) spectroscopy, which have proven to be very helpful for developing models to ascertain and describe the structure of the various gels formed.[17]

For the first time, this work aims to investigate the reasons why Raman spectroscopy is much more rarely employed with respect to the other above-mentioned techniques, especially if geopolymers are considered.[18–31] This is reported to be due to high levels of fluorescence when shorter excitation wavelengths are used and to the appearance of photoluminescence bands when longer ones are preferred.[18] On the other hand, it must be considered that the silicate tetrahedron highly covalent character would make Raman spectroscopy theoretically one of the ideal techniques for these materials investigation.[18,19]

To the authors' knowledge, only two papers systematically take into account the Raman contribution to the geopolymers study.[19,20] Their Raman spectra are considered by Kosor et al.[19,20] in the same way as those of silicate glass, evaluating the silicate tetrahedra polymerization degrees present in the spectra. The Geopolymerization Index (GI), ranging between 0 and 1, is defined for fly ash geopolymers as the ratio between the integral of the normalized Raman spectrum of α-quartz and that of the investigated sample in the spectral region between 300 and 1200 cm^{-1}.[19] The Geopolymer Depolymerization Index (GDI) is instead proposed[20] as a measure of the depolymerized tetrahedra content and is defined as the ratio between the integrals of the 800–1200 and the 300–500 cm^{-1} regions, based on the same concept as the glass polymerization index.[32] In fly ash activated with sodium silicate solutions[19,21] and in fly ash pastes modified with graphene oxide,[21] the appearance of broad signals centered around 835, 940, 990, 1060, and 1160 cm^{-1} is reported and attributed, respectively, to Q^0, Q^1, Q^2, Q^3, and Q^4 silicate tetrahedron units positions. In the Q^n notation,[33] Q stands for the Si atom and n (0–4) indicates the number of bridging oxygen atoms.[34] The appearance of a peak at 1064 cm^{-1} is confirmed also for metakaolin-based AAMs[22]: in this case, the signal is sharp; nevertheless, the authors assign it to Si–O^- vibration where O^- denotes a nonbridging oxygen within a Q^3 or Q^2 unit, ruling out a possible assignment of the peak to carbonate species, because it was found also on products activated with KOH and NaOH only. On the other hand, when waterglass is employed as activator, the possibility of a carbonate contaminant generating this band must be taken into account[35] together with the eventual crystallization of efflorescences on mature products.[36,37]

A misunderstanding that apparently leads to results concerning the metakaolin-based AAMs aluminosilicate structure is that concerning the band at 143 cm^{-1} and

those at 400, 514–520, and 635–640 cm^{-1}: the former has been attributed to intratetrahedral vibrations of polymerized silicate tetrahedra,[23] and the two latter to T-O-T (T: Si or Al) bending and T-O symmetric stretching modes.[23,24] Nevertheless, these four signals must be most probably assigned to anatase present in the raw materials.[38]

Another specific application of Raman[25] or FT-Raman[18,26] spectroscopy to geopolymers study is that of investigating the material hydration detecting the hydroxyl bonds vibrations in the high wavenumber region of the spectra, also with the aid of mapping.[25]

Other employs of Raman spectroscopy in this field are rather occasional, restricted to graphite[27] or graphene[28,29] analysis, or limited to answer specific questions such as detecting calcium activity in geopolymer paste[30] or testing the efficiency of photoactive TiO_2 incorporation.[31]

The present work origins from the contradiction between the theoretical potential of Raman spectroscopy in the investigation of geopolymers and its limited use, often with debatable results. Therefore, filling a gap in the literature, it aims to systematically reconsider its suitability in the application to AAMs study, starting from new data about geopolymers made with metakaolin, volcanic materials, clay sediments, and ceramic wastes precursors. This is done comparing the results obtained on the precursors and on the respective AAMs, both the mature ones (more than 28 days after synthesis) and the fresh ones immediately after synthesis, followed during the first 8 h of the geopolymerization process.

2 | MATERIALS AND METHODS

2.1 | Materials

2.1.1 | Raw materials

In the present study, different aluminosilicate raw materials have been selected for the preparation of AAM products (Figure 1):

- Commercial metakaolin (ARGICAL™ M-1000 supplied by IMERYS, France) used either alone or in combination with the other aluminosilicate precursors. Metakaolin (hereafter labeled MK) was used without any treatment.
- Three Sicilian volcanic deposits: (i) Aeolian pumice, sampled in the dismissed quarry of Porticello (Aeolian Islands, Sicily, Italy); (ii) volcanic ashes from 2013 Mt. Etna paroxystic events, collected in the local landfill on the south-east slope of the volcano (Santa Venerina, Sicily, Italy); (iii) volcanic paleo-soils, locally known as "ghiara", having composition similar to Etnean ashes and a characteristic reddish color,[39] sampled by hand shovel in a volcanic tunnel in the south slope of Mt. Etna (Sicily, Italy).
- All these raw materials were water-washed and dried before dry milling (<75 μm).
- Sicilian clay sediments sampled in Poggio Safarello (central southern Sicily, Italy) where mainly Plio-Quaternary sediments are exposed. Once sampled, clay raw materials were calcined at 800°C for 3 h in order to improve their reactivity toward geopolymerization reaction.[40] Finally, they were dry milled to select only grain size <15 μm.
- Tiles waste provided by "La Bottega Calatina" (LBC), a Sicilian industry of painted tiles. The broken tiles or those showing imperfections are usually disposed as nontoxic material and have been selected for the purpose of this study as industrial by-products. The fragments have been retrieved, the glaze removed, and then finely ground (approximately 10 μm).

All the precursors mentioned above have aluminosilicatic composition and amorphous fraction, both necessary for the production of geopolymers. These raw materials were analyzed before their use as precursors in alkaline activation; their chemical and mineralogical results are reported in previous works[36,37,41,42]; the latter are summarized in Table S1, whereas SiO_2/Al_2O_3 ratios are reported in Table S2.
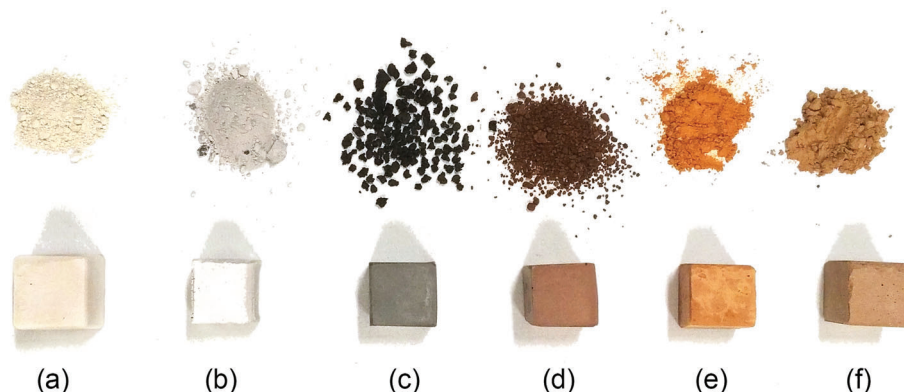
FIGURE 1 (a) Metakaolin, (b) pumice, (c) volcanic ash, (d) ghiara, (e) clay, and (f) LBC ceramic waste precursors (top) and respective representative AAMs (bottom) [Colour figure can be viewed at wileyonlinelibrary.com]

(a)   (b)   (c)   (d)   (e)   (f)

- Laboratory grade sodium hydroxide (8M), potassium silicate (molar ratio 0.65 Si/K), commercially known as Geosil 14515 (provided by Wollner), and sodium silicate (molar ratio $SiO_2/Na_2O = 3$) (provided by Ingessil s.r.l., Italy) solutions alone or in mixture have been used as alkali activators.

2.1.2 | Alkali-activated materials

In this paragraph, the alkali activation procedures are briefly exposed; details concerning each studied formulation are reported in Table 1.

A formulation made only of metakaolin has been prepared, and the activated product has been analyzed. This MK-based binder has a much simpler composition compared with the other AAMs produced from multiphase raw materials (Table S1) and is necessary as reference and comparison.

All aluminosilicate precursors have been used either alone or in binary mixtures with small additions of MK (10–20 wt%).

Solid mixtures were then activated with Na_2SiO_3 and NaOH or K_2SiO_3 solutions, choosing among the best formulation.[36,37,41,43]

The slurries were mechanically mixed for 5 min, poured into molds, and then cured at room temperature ($22 \pm 3°C$) for 28 days, covered by a thin polymer film to maintain a constant level of moisture. This condition could not be maintained for the products analyzed soon after synthesis, which were exposed to air during the Raman analyses.

2.2 | Methods

Preliminary tentative investigations with a portable instrumentation with handheld measuring head

TABLE 1 Details of alkali-activated materials formulations

Precursor	AAMs label	Precursor/MK ratio (wt%)	NaOH/Na$_2$SiO$_3$ (wt%)	Liquid/solid ratio[a]
Metakaolin	MK-GP	0/100	50/50	0.68
Pumice	POM 1-30	70/30	50/50	0.72
Volcanic ash	Na-VM10	90/10	37.5/62.5	0.32
	Na-VM20	80/20	37.5/62.5	0.32
	VM1-10	90/10	23/77	0.52
	VM1-20	80/20	23/77	0.52
	K-VM10	90/10	0/100	0.31
	K-VM20	80/20	0/100	0.31
Ghiara	Na-GM10	90/10	37.5/62.5	0.32
	Na-GM20	80/20	37.5/62.5	0.32
	GM1-10	90/10	27/73	0.44
	GM1-20	80/20	27/74	0.44
	K-GM10	90/10	0/100	0.31
	K-GM20	80/20	0/100	0.31
Clay	PS3	0	23/77	0.52
LBC ceramic waste	LBCa30-70	100	30/70	0.45
	LBCa30-70+10	90/10	30/70	0.45
	LBCa30-70+20	80/20	30/70	0.47
	LBCa50-50	100	50/50	0.44
	LBCa50-50+10	90/10	50/50	0.43
	LBCa50-50+20	80/20	50/50	0.45
	LBCa70-30	100	70/30	0.43
	LBCa70-30+10	90/10	70/30	0.44
	LBCa70-30+20	80/20	70/30	0.44

[a]Liquid to solid ratio is referred to the ratio between the alkali solution and the solid precursor.

(i-Raman® Plus spectrometer [B&W Tek], equipped with a 785 nm diode laser) were carried out.

Nevertheless, the analyses were mainly conducted with a fixed micro-Raman instrumentation, a Jasco NRS3100 spectrometer equipped with a Notch filter and a Peltier-cooled ($-49°C$) 1024×128 CCD. In this work, the 532-nm excitation wavelength was employed, reaching, with the 1800 g/mm grating, a spectral resolution of ~3 cm^{-1}. The calibration of the system was verified using the 520.7-cm^{-1} Raman band of silicon before each experimental session.

Precursors and mature—more than 28 days—AAMs were analyzed for all the groups of considered materials. In order to achieve the wider analytical representativity possible, 10 spectra per each powdered sample were acquired on different spots employing an Olympus (Japan) $20\times$ objective (N.A. = 0.45), with a spatial resolution of about 4 μm. The laser power value was controlled through optical density filters and kept around 1 mW on the sample to avoid heating effects. Time and number of accumulations were regulated according to the sample response. Both the low wavenumber region (130–1200 cm^{-1}) and the high one (3100–3700 cm^{-1}) were investigated.

For clay and LBC ceramic waste, measurements during the geopolymerization process were also carried out. A small quantity of powders of the two precursors were alkali activated (see Section 2.1.2) and, immediately after, analyzed using an Olympus (Japan) $50\times$ LWD objective (N.A. = 0.50) in the 130–1200 cm^{-1}. The laser power was set at ~1.5 mW, the time at 60 s, and the accumulations at 10. At the end of each 10-min measurement, a minimal adjustment of the focus was done and a new spectrum was started, for a total of 8 h.

In general, the spectra are presented as such, with the aim of providing an accurate idea of the Raman

TABLE 2 List of the signatures found in the different materials of the present work and respective attributions

| Signals (cm^{-1}) | Attribution | Materials | | Ref. |
		Precursors	AAMs	
150, 200, 395, 518, 638	Anatase	MK, CL	MK, PM, VA, GA, CW	Murad[38]
620	Rutile		VA	Lafuente et al.[44]
327, 392, 525, 560, 666, 770, 1009	Augite/diopside	PM	VA, GA	Minčeva-Šukarova et al.[45]
461	Quartz		PM, CW	Lafuente et al.[44]
480, 505	Anorthite	VA	GA	Lafuente et al.[44]
823, 855	Olivine	VA	VA, GA	Kuebler et al.[46]
224, 244, 292, 408, 500, 606	Hematite	GA, CL, CW	GA, CL	Froment et al.[47] and dos Santos et al.[48]
730	Maghemite	GA	VA, GA	Froment et al.[47] and Tanevska et al.[49]
660–673	Magnetite	VA, GA, CL, CW	VA, GA, CL, CW	Froment et al.[47]
	Disordered hematite (Al-for-Fe substitution in hematite; hematite recrystallization)			Zoppi et al.,[50] Leon et al.,[51] and Marshall et al.[52]
680–690	Spinel-like mineral belonging to the ferrite group	VA	VA	D'Ippolito et al.[53]
960–1000, 1062–1068	Q^2, Q^3 (silicate tetrahedron)		PM, VA, GA, CL, CW	Kosor et al.[19,20] and Xu et al.[21]
488, 790	Si–O–Si Bending, Q^0 (silicate tetrahedron)	PM		Colomban[32,54]
1045, 1100	Q^3 (silicate tetrahedron)	GA		Kosor et al.[19] and Arnoult et al.[55]
3440	OH stretching vibrations		CL, CW	Szechyńska-Hebda et al.,[18] Steinerová and Schweigstillová,[25] and Mierzwiński et al.[26]
3630	Si-OH		CW	Walrafen[56]

Note: MK: metakaolin; PM: pumice; VA: volcanic ash; GA: ghiara; CL: clay; CW: LBC ceramic waste.

spectroscopy performance if applied to AAMs analysis in the above-mentioned conditions.

3 | RESULTS

The preliminary results obtained with the portable instrumentation and 785-nm excitation indicated that these conditions seem not suitable for the purpose of the work, due both to the wavelength employed and to instrumental features: mainly photoluminescence bands and filter-connected noise were obtained, together with fluorescence.

The results will be therefore focused on micro-Raman analyses results. They will be reported directly comparing the data obtained on the precursors (grey spectra) and those of the respective AAMs (black or colored spectra), divided according to the raw material. The principal Raman signatures found are listed in Table 2.

3.1 | Metakaolin

Metakaolin was employed in the synthesis of the AAMs, as main constituent (MK-GP) or as additive in different percentages with the exception of the clay-based products (Table 1). Therefore, the results obtained for this precursor are particularly important since they can affect those relative to many other materials involved in this study. They are shown in Figure 2a, clearly displaying the signals of anatase at about 150, 200, 395, 518, and 638 cm^{-1} both in the raw material and in the representative spectrum of the reacted product.[38] Actually, the producer reports 1.5 wt% of TiO_2 in the used metakaolin. It is well known that anatase's large Raman cross section, due to

the high polarizability change with change of normal coordinate of its covalent bonds,[57] allows its revelation with this technique even if present in very low amounts. In this case, its high intensity signal constitutes a drawback because it can hinder the observation of the other contributions and is at the basis of the here-confirmed above-mentioned misinterpretations.[23,24]

3.2 | Pumice

The representative spectra relative to pumice raw material and respective AAM with metakaolin addition are shown in Figure 2b. Pumice exhibits signals of both a crystalline and an amorphous phase. The former is evident in the pyroxene (augite/diopside) bands at 327, 392, 525, 560, 666, 770, and 1009 cm^{-1},[45] confirming the augite identification by XRD[36,37] (see also Figure S1). On the other hand, the broad bands centered at 488 and 790 cm^{-1} could be ascribed to the glassy phase: the much higher intensity of the approximately 500- cm^{-1} signal, ascribed to the bending vibration of Si–O–Si bond, with respect to the stretching one at about 1000 cm^{-1}, is typical of highly connected structures.[32,54]

The representative AAM spectrum includes signals due to metakaolin-linked anatase and to quartz (461 cm^{-1})[44] as well as two bands at about 1000 and 1064 cm^{-1}. These two are reported as the Q^2 and Q^3 spectral components of the silicate tetrahedra units vibrations in the fly ash geopolymers.[19–22] Nevertheless, the finding of sodium carbonates like trona ($Na_2CO_3NaHCO_3\cdot2H_2O$) by means of X-ray diffraction (XRD) in this sample[36] (see also Figure S1) could question the attribution of the latter signal. The compound constituting this efflorescence is in fact characterized by a strong band at about 1067 cm^{-1}.[58]

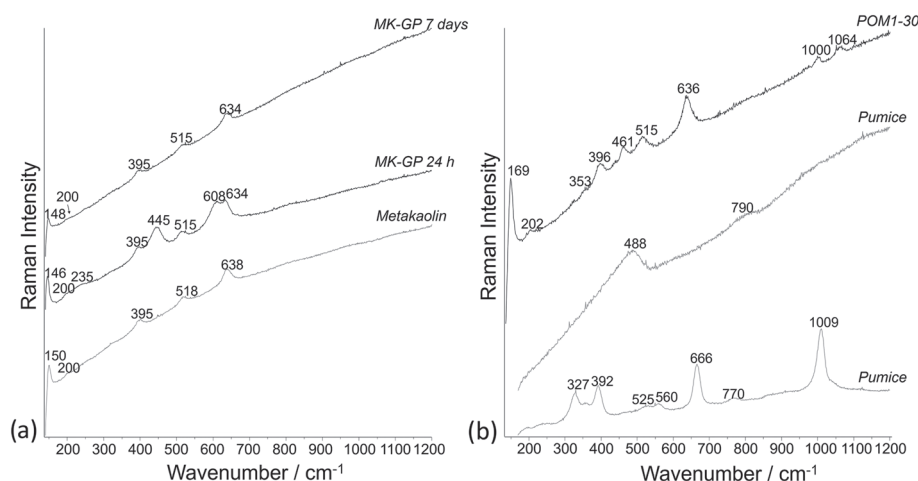**FIGURE 2** Representative Raman spectra of (a) metakaolin and (b) pumice precursors and respective AAMs; spectra are stacked for clarity

3.3 | Volcanic ash

More variable results were obtained for volcanic ash precursor and products, respectively, shown in Figure 3a,b. The Raman spectra of the raw material exhibit the signals related to augite (Table 2), anorthite (480, approximately 505 cm^{-1}),[44] and weak bands of olivine (820, 855 cm^{-1}),[46] confirming XRD results[37,41] (see also Figure S1). Also, hematite/magnetite or amorphous iron oxide (288, 405, 665 cm^{-1})[48] and a broad band around 680 cm^{-1} are recurring. The latter attribution to a spinel-like mineral belonging to the ferrite group is likely.[53]

The spectra shown for the AAM (Figure 3b) are representative of the results obtained for the different studied formulations (Table 1). Mainly, mineral phases are revealed (Table 2): augite was found in all the products except VM1-20, which is instead characterized by metakaolin-related anatase signals. Hematite and rutile signals are found especially in Na-VM10; furthermore,

the bands DB1 and DB2 of olivine with their resolution, position and intensity ratio point to a magnesian olivine close to the forsterite endmember.[46] Anorthite (Table 2) and maghemite (main band at 730 cm^{-1})[47,49] signatures are visible in addition in the spectra of K-VM20. A broad band ranging between 680 and 690 cm^{-1} is recurring in all the samples. Furthermore, the probable Q^2 and Q^3 related bands[19–22] already highlighted for pumice AAM could be revealed at about 1000 and 1064 cm^{-1} in two of the spectra acquired on the different specimens.

3.4 | Ghiara

Both ghiara raw material and AAMs Raman spectra (Figure 4a,b, respectively) are dominated by iron oxides signature. In ghiara spectra, hematite signals (224, 244, 292, 408, 500, 606 cm^{-1})[47] are associated to the band at 660 and that around 730 cm^{-1}, respectively, attributable to magnetite[47] and maghemite.[47,49] The assignment of

FIGURE 3 Representative Raman spectra of (a) volcanic ash precursor, (b) respective AAMs; spectra are stacked for clarity

FIGURE 4 Representative Raman spectra of (a) ghiara precursor, (b) respective AAMs; spectra are stacked for clarity

the former is debated[52]: it generally appears in polycrystalline, nanostructured, and doped hematite and is presently ascribed to disorder-induced breaking of the symmetry properties[52] due to Al-for-Fe substitution in hematite[50] or its recrystallization with high temperature.[51] Anorthite and augite signals, confirming XRD results,[37,41] are also visible together with those of magnesian olivine (Table 2). The 1045- and 1100-cm^{-1} bands could be due to the silicate Q^3 components[19,55] accounting for the amorphous part of this soil.[37]

In the ghiara AAMs, mainly the signals of the same minerals as those characterizing the precursors (anatase, augite, olivine, anorthite, hematite, magnetite, maghemite; Table 2) were found recurrently in almost all the studied samples.

Apart from these, an ill-defined broad band located at about 1064 cm^{-1} was sometimes detected in spectra of the Na-GM10 and K-GM10 formulations (Table 1) accounting for the amorphous phase formation[19–22]: this band is clearly different in shape and position from the above-mentioned respective ones visible in the raw material spectrum.

3.5 | Clay

The Raman results on calcined clay and respective AAM are reported in Figure 5a. The shown spectra are noisier with respect to the other analyzed materials; most of those acquired are characterized by a stronger fluorescence: the compromise between quality and time of acquisition was more difficult to be achieved. Due to the low polarizable character of aluminosilicatic bonds in the clay lattice[59] giving weak Raman scattered signal

and overlapping fluorescence,[60] it is well known that Raman spectroscopy is not the ideal technique to be employed for clay minerals analysis.

Nevertheless, in the calcined precursor, the signals of hematite can be recognized—being iron oxides characterized by more covalent bonds[59]—together with those of anatase (Table 2); hematite is revealed in the clay-AAM too. The latter exhibits in addition a band at approximately 960 cm^{-1}, probably to be ascribed to the silicate tetrahedron Q^2 unit[21]: its shift toward lower wavenumbers may be due to the presence of aluminum in the silicate network[61]; it is not possible to state if other spectral components are present due to the low signal to noise ratio.

This AAM was monitored continuously for 8 h starting immediately after the alkaline activation of the calcined clay (see Section 2.2). Figure 5b exemplifies the results showing only the spectra where a change could be highlighted. After 100 min, quartz main signal (blue line) appears together with those of anatase (red lines). Hematite signature presence is rather constant, whereas the other two minerals appear and disappear over the hours. Rather than to a temporal evolution, this seems to be due to micrometric movements of the gel during its polycondensation, also enhanced by the laser excitation. The employ of a 50× LWD objective worsened the representativity of the results; on the other hand, contact of the objective with the corrosive substance must be avoided. Furthermore, trials with both lower magnification objectives and handheld probes demonstrated that no Raman spectrum at all could be obtained. Starting from 370 min after synthesis, the fluorescence background is remarkable and the Raman signals become barely readable.
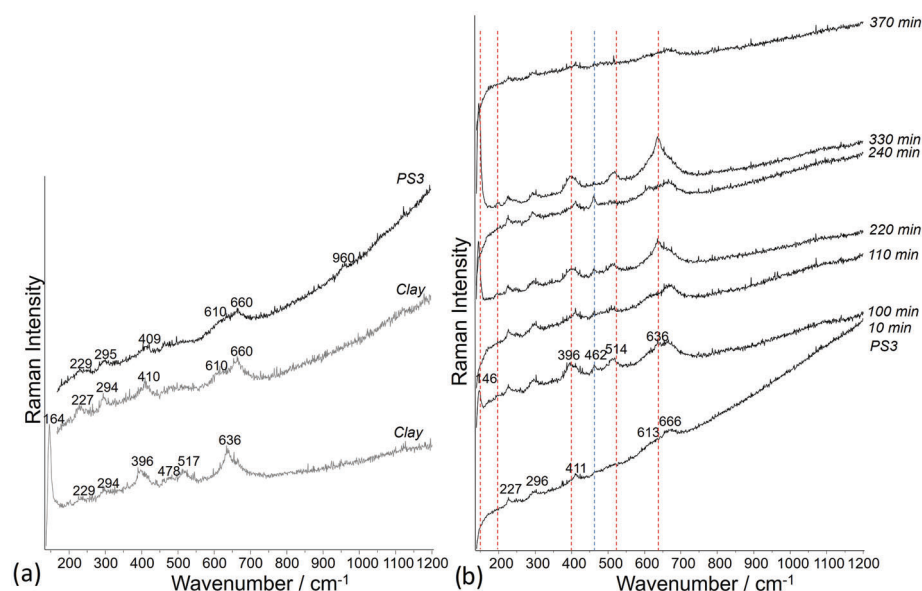
FIGURE 5 Representative Raman spectra of (a) clay precursor and respective AAM, (b) AAM during geopolymerization; spectra are stacked for clarity [Colour figure can be viewed at wileyonlinelibrary.com]

Finally, the Raman analysis performed in the high wavenumber region (3100–3700 cm^{-1}) highlighted a difference between the spectrum of the raw material and that of the respective mature AAM (Figure S2). The band at approximately 3440 cm^{-1} already attested in AAMs analysis with Raman[25] and FT-Raman spectroscopy[18,26] and attributed to OH stretching vibrations is visible in the reacted product.

3.6 | LBC ceramic waste

Representative Raman results obtained on the ceramic precursor and the different AAM formulations (Table 1) are reported in Figure 6. Once again, hematite signature is recurrent; the samples including metakaolin, as expected, show anatase signals too. Attention must be paid to the band ranging from 460 to 471 cm^{-1} connected to quartz: according to Kosor et al.[19] its broadening and shift would hint to the formation of a differently structured aluminosilicate material. This is evident especially in the case of LBCa30-70 where it appears broadened and shifted to 456 cm^{-1} and connected to the 615 cm^{-1} band, whose intensity excludes its association to hematite. It could be due instead to the broken Si–O–Si bonds of siloxane rings vibrations.[19] The 456- cm^{-1} band is too shifted to ascribe these signals to rutile; furthermore, no evidence of TiO$_2$ came from XRD analyses that are being carried out on precursors and products. Almost all the spectra exhibit a band between 1062 and 1068 cm^{-1}, together with a weaker one around 970 cm^{-1}. Once
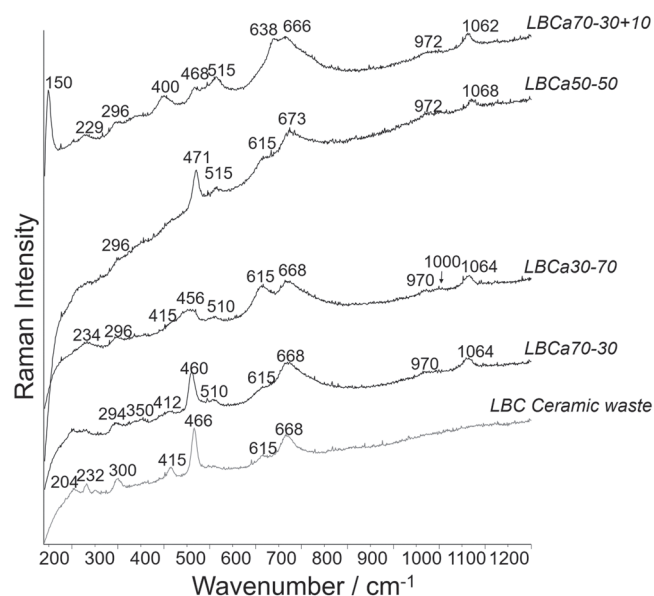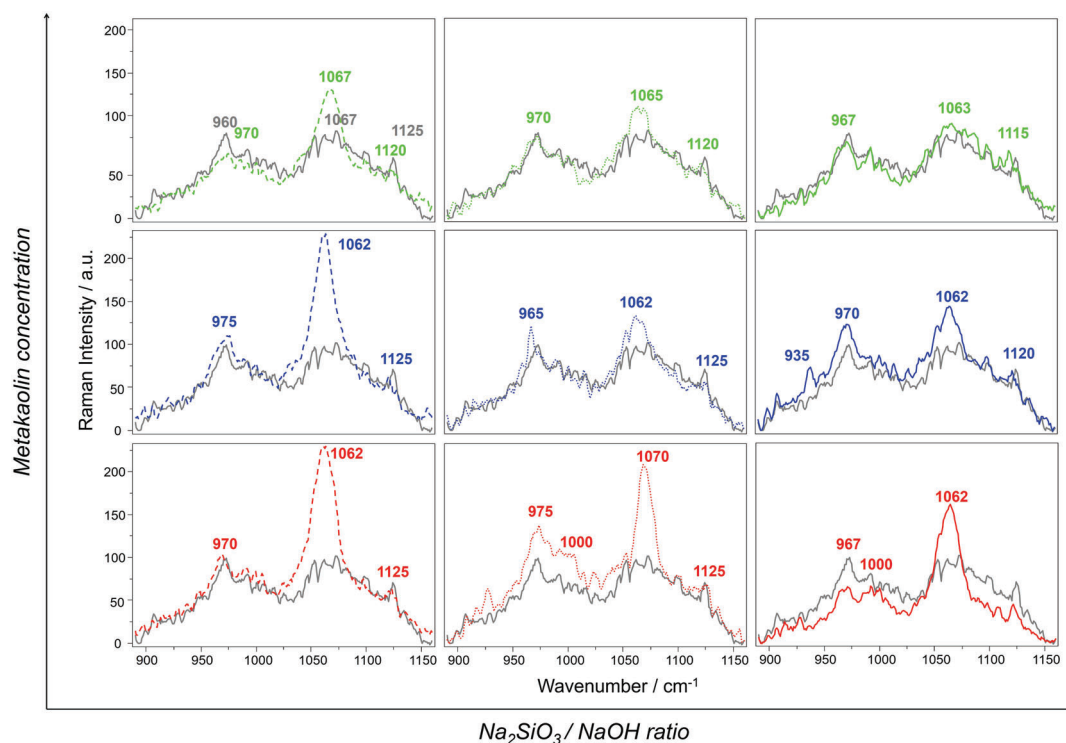

FIGURE 6 Representative Raman spectra of LBC ceramic waste precursor and respective AAMs; spectra are stacked for clarity

again, the attribution to Q^3 and Q^2 type stretching vibration of the silicate tetrahedron with aluminum presence can be hypothesized.[19–22,61] On the other hand, the finding by means of in progress XRD measurements of small quantities of thermonatrite (Na$_2$CO$_3$·H$_2$O), which is reported to display its principal peak at about 1067 cm^{-1}, could question this attribution.[58]

Considering the most diffused interpretation of these bands in the literature connected to geopolymers involving aluminosilicate structure, a focus on the region between 890 and 1160 cm^{-1} was carried out comparing the ceramic precursor and the different AAMs formulations (Figure 7). These spectra were baseline-subtracted in the same way with LabSpec software using linear segments. The 1062–1070 cm^{-1} band is observed to lose relative intensity going from the AAMs without metakaolin addition to those with 20% MK; the same trend is visible with the increase of waterglass percentage with respect to NaOH in the activators mixture. If the approximately 1065- cm^{-1} band is associated to Q^3 units,[19–22] it must be deduced that samples activated with a higher percentage of NaOH and those with 0% or 10% MK in the precursor perform a higher structural crosslinking. Furthermore, it can be noted how sample LBCa30-70 spectrum does not exhibit the shoulder at approximately 1120 cm^{-1} characterizing all the other materials and probably to be attributed to Q^4 units.[55]

LBCa30-70+20 (Table 1) was chosen to carry out Raman analyses during geopolymerization because it displayed the shortest setting time. The most significative results are shown in Figure 8. The spectrum of the material 10 min after its synthesis shows a 970-cm^{-1} band, connected to Q^2 units[19–22,61] and a much weaker one at 1044 cm^{-1}; the latter must be due to the used activating solution with maximum at approximately 1038 cm^{-1}. Similarly, to the process observed for the clay-AAM, the first evidence of quartz (460 cm^{-1}, blue line) appears after 90 min, whereas anatase alternating presence (red line) could be due to the already highlighted problems connected to the very high spatial resolution and the sample micromovements during setting. Once again, after 370 min, the spectrum flattens and, as visible in Figure 8b where the spectra are shown without stacking, fluorescence gradually increases with time. It can be hypothesized that at this moment, the different processes involved in the geopolymerization mechanism take place at the same time.

The analyses performed in the high wavenumber region on mature samples (Figure S2) highlighted the appearance of the OH stretching band at 3440 cm^{-1} in LBCa70-30+20,[18,25,26] better visible in LBCa70-30, and of the 3630 cm^{-1} one in LBCa50-50+20. The latter could account for Si-OH cohesive interactions similar to the nonhydrogen-bonded OH groups in liquid water.[56]

FIGURE 7 Representative baseline-subtracted Raman spectra in the 890–1160 cm^{-1} region of LBC ceramic waste precursor (in grey) and respective AAMs (red: no MK addition; blue: 10% MK; green: 20% MK; dashed: NaOH/Na$_2$SiO$_3$ = 70/30; dotted: NaOH/Na$_2$SiO$_3$ = 50/50; full: NaOH/Na$_2$SiO$_3$ = 30/70) [Colour figure can be viewed at wileyonlinelibrary.com]
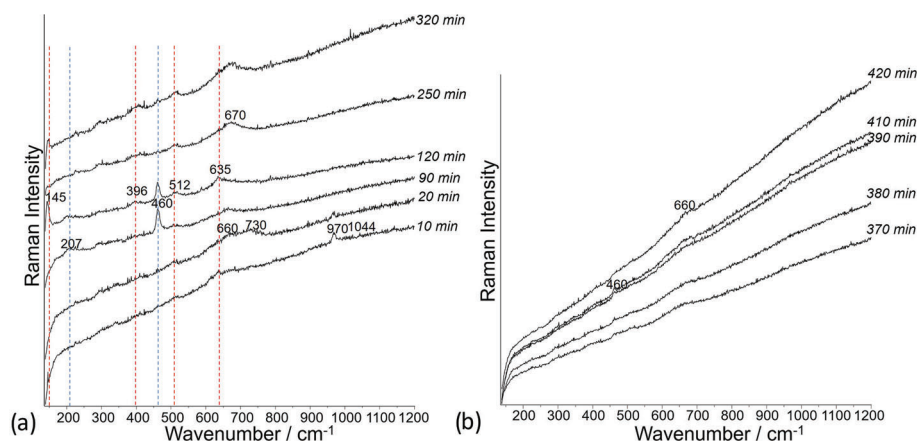
FIGURE 8 Representative Raman spectra of LBCa30-70+20 during geopolymerization; in (a) spectra are stacked for clarity [Colour figure can be viewed at wileyonlinelibrary.com]

4 | DISCUSSIONS

The analysis of the results obtained on the different groups of materials leads to several remarks concerning the detection of the mineral phases and of the amorphous material.

The acquisition of 10 spots on the homogenized powders with a 532-nm excitation wavelength and an approximately 4-μm spot size allowed a good reconstruction of the mineralogical compositions of volcanic ash and ghiara precursors and AAMs, confirming those obtained by XRD[37,41] (see also Figure S1). This is not the case for clay- and ceramic-based materials where the spectra acquired with the green laser are mainly dominated by hematite signature: this dissuades from the use of a red laser for the analyses, because it would further enhance its revelation to the detriment of the aluminosilicatic phases. Another obstacle to the thorough comprehension of these materials can be anatase presence in metakaolin, strongly affecting the spectra acquired on all materials that contain it, even at concentrations as low as 0.1 wt%.

It is clear that the GI,[19] proposed for fly ash geopolymers, cannot always be applied as indicator of a good geopolymerization. An example is given by volcanic ash AAMs, where no evident quartz signals were revealed

(see Figure 3b) notwithstanding the already demonstrated[37,41,43] good quality of these products. Furthermore, quartz revelation can be hindered by other signatures, and, being the representativity of micro-Raman analyses low, the results strictly depend on the analyzed spot.

The most suitable molecular spectroscopic technique employed to ascertain that the geopolymerization process occurred seems to be the infrared one: its efficiency was earlier proved on some of the materials object of this work.[36,37,41] Nevertheless, the amorphous components detected with Raman analyses for all the analyzed groups of AAMs—though in a small percentage of the total number of spectra—can be considered an indication of occurred transformation in the aluminosilicate structure. Even if the samples do not show visible efflorescences, a doubt with the assignment of the 1065-cm^{-1} band to carbonate efflorescences should be taken into account. However, for the LBC ceramic-based products, a correlation between the spectral components (position/relative intensity) in the region 890–1160 cm^{-1} and the different formulations could lead to useful indications about their final local structure. The latter is indeed strongly dependent on the reactivity of the raw materials but also on the mix design (raw materials and alkali solution proportion); therefore, it can preliminarily suggest if the chosen parameters lead toward a more or less crystalline or amorphous product. The GDI[20] seems difficult to be applied to the materials here investigated, because the region between 300 and 500 cm^{-1} is often strongly affected by signals of various mineral phases so that the amorphous aluminosilicate bending band is rarely visible.

The hydroxyl group revelation in the high wavenumber region of the spectra was successful only for clay- and LBC ceramic-based materials, and it was proven to be an interesting application when information about the degree of AAM hydration is required.

The Raman analyses during the first 8 h of geopolymerization seems not applicable in these conditions, whereas it proved to be effectively carried out by means of attenuated total reflectance Fourier transform infrared spectroscopy (FTIR-ATR).[41] It should be performed with much higher laser power to avoid the use of high magnification objectives, taking into account important parameters such as illuminated area, volume, water presence, and porosity that could control the risk of laser-induced local heating effects.

5 | CONCLUSIONS

It can be concluded that this work was useful to reconsider literature concerning Raman spectroscopy application to low-calcium AAMs or geopolymers, in the light of new data. Raman spectra of this kind of products based on volcanic raw materials, clay, and ceramic wastes were reported for the first time.

These helped to highlight both advantages and drawbacks of this technique. On one hand, the different kinds of answers that can be provided were pointed out, such as the simultaneous detection of crystalline and amorphous portions, the latter providing information on the reaction degree. On the other hand, the technical and instrumental problems that could hinder its wider usage in the field were clarified, such as representativity issues. Raman spectroscopy can provide data concerning mineral composition and aluminosilicate species cross-linking in relation to the AAM formulation. Nevertheless, the common presence of both crystalline and glassy phases in geopolymer matrices can generate some problems of analytical representativity, especially if micro-Raman is employed. A possible future development of the work would be to test portable Raman with 532-nm excitation wavelength.

ORCID
Maria Cristina Caggiani https://orcid.org/0000-0001-8475-1175
Alessia Coccato https://orcid.org/0000-0002-6641-2820
Germana Barone https://orcid.org/0000-0003-0822-2436
Claudio Finocchiaro https://orcid.org/0000-0002-8841-283X
Maura Fugazzotto https://orcid.org/0000-0002-9636-6896
Gabriele Lanzafame https://orcid.org/0000-0001-5352-9918
Roberta Occhipinti https://orcid.org/0000-0001-8220-0943
Antonio Stroscio https://orcid.org/0000-0002-7625-829X
Paolo Mazzoleni https://orcid.org/0000-0002-7281-923X

REFERENCES
[1] J. Davidovits, *J. Therm. Anal.* **1991**, *37*, 1633.
[2] *Alkali Activated Materials: State-of-the-Art Report, RILEM TC 224-AAM* (Eds: J. L. Provis, J. S. J. van Deventer), Vol. 13, Springer Science & Business Media, Dordrecht **2014**.

[3] C. Shi, A. F. Jiménez, A. Palomo, *Cem. Concr. Res.* **2011**, *41*, 750.

[4] A. Palomo, P. Krivenko, I. Garcia-Lodeiro, E. Kavalerova, O. Maltseva, A. Fernández-Jiménez, *Mater. Construcción* **2015**, *64*(315), e022. https://doi.org/10.3989/mc.2014.00314

[5] C. Shi, B. Qu, J. L. Provis, *Cem. Concr. Res.* **2019**, *122*, 227.

[6] J. L. Provis, *Cem. Concr. Res.* **2018**, *114*, 40.

[7] P. Colomban, *Ceramics* **2020**, *3*(3), 312.

[8] M. Rowles, B. O'Connor, *J. Mater. Chem.* **2003**, *13*, 1161.

[9] P. Duxson, J. L. Provis, G. C. Lukey, S. W. Mallicoat, W. M. Kriven, J. S. J. Van Deventer, *Colloids Surfaces a Physicochem. Eng. Asp.* **2005**, *269*, 47.

[10] S. A. Bernal, E. D. Rodríguez, A. P. Kirchheim, J. L. Provis, *J. Chem. Technol. Biotechnol.* **2016**, *91*, 2365.

[11] J. L. Provis, A. Palomo, C. Shi, *Cem. Concr. Res.* **2015**, *78*, 110.

[12] J. L. Provis, G. C. Lukey, J. S. J. Van Deventer, *Chem. Mater.* **2005**, *17*, 3075.

[13] J. L. Provis, S. A. Bernal, *Annu. Rev. Mater. Res.* **2014**, *44*, 299.

[14] A. Fernández-Jiménez, A. Palomo, M. Criado, *Cem. Concr. Res.* **2005**, *35*, 1204.

[15] H. Xu, J. S. J. Van Deventer, *Colloids Surfaces a Physicochem. Eng. Asp.* **2003**, *216*, 27.

[16] C. A. Rees, J. L. Provis, G. C. Lukey, J. S. J. Van Deventer, *Langmuir* **2007**, *23*, 8170.

[17] F. Pacheco-Torgal, J. Labrincha, C. Leonelli, A. Palomo, P. Chindaprasit, *Handbook of Alkali-Activated Cements, Mortars and Concretes*, Elsevier, Amsterdam **2014**.

[18] M. Szechyńska-Hebda, J. Marczyk, C. Ziejewska, N. Hordyńska, J. Mikuła, M. Hebda, *IOP Conf. Ser.: Mater. Sci. Eng.* **2019**, *706*, 012017.

[19] T. Kosor, B. Nakić-Alfirević, A. Gajović, *Vib. Spectrosc.* **2016**, *85*, 104.

[20] T. Kosor, B. Nakić-Alfirević, S. Svilović, *Vib. Spectrosc.* **2016**, *86*, 143.

[21] G. Xu, J. Zhong, X. Shi, *Fuel* **2018**, *226*, 644.

[22] C. H. Rüscher, E. Mielcarek, J. Wongpa, F. Jirasit, W. Lutz, New Insights on Geopolymerisation Using Molybdate, Raman, and Infrared Spectroscopy, Strategic Materials and Computational Design (Eds: W. M. Kriven, Y. Zhou, M. Radovic, S. Mathur, T. Ohji), The American Ceramic Society, Westerville **2010**, pp. 31,10.

[23] K. Brylewska, P. Rożeka, M. Króla, W. Mozgawa, *Ceram. Int.* **2018**, *44*, 12853.

[24] L. Zhang, F. Zhang, M. Liu, X. Hub, *Chem. Eng. J.* **2017**, *313*, 74.

[25] M. Steinerová, J. Schweigstillová, *Ceramics – Silikáty* **2013**, *57*(4), 328.

[26] D. Mierzwiński, M. Łach, M. Hebda, J. Walter, M. Szechyńska-Hebda, J. Mikuła, *J. Therm. Anal. Calorim.* **2019**, *138*, 4167.

[27] J. Huang, Z. Li, J. Zhang, Y. Zhang, Y. Ge, X. Cui, *Chem. Eng. J.* **2020**, *397*, 125528.

[28] A. Amri, Y. B. Hendri, E. Malindo, M. M. Rahman, *J. Phys.: Conf. Ser.* **2019**, *1351*, 012101.

[29] N. Lertcumfu, P. Jaita, S. Thammarong, S. Lamkhao, S. Tandorn, C. Randorn, T. Tunkasiri, G. Rujijanagul, *Colloid. Surfaces a* **2020**, *602*, 125080.

[30] E. I. Diaz, E. N. Allouche, S. Eklund, *Fuel* **2010**, *89*, 992.

[31] J. R. Gasca-Tirado, A. Manzano-Ramírez, C. Villaseñor-Mora, M. S. Muñiz-Villarreal, A. A. Zaldivar-Cadena, J. C. Rubio-Ávalos, V. Amigó Borrás, R. Nava Mendoza, *Micropor. Mesopor. Mat.* **2012**, *153*, 282.

[32] P. Colomban, *J. Non-Cryst. Solids* **2003**, *323*, 180.

[33] G. Engelhardt, D. Zeigan, H. Jancke, D. Hoebbel, Z. Weiker, *Z. Anorg. Allg. Chem.* **1975**, *418*, 17.

[34] L. Vidal, E. Joussein, M. Colas, J. Cornette, J. Sanz, I. Sobrados, J.-L. Gelet, J. Absi, S. Rossignol, *Colloid. Surface. A* **2016**, *503*, 101.

[35] I. Halasz, M. Agarwal, R. Li, N. Miller, *Catal. Letters* **2007**, *117*, 34.

[36] R. Occhipinti, A. Stroscio, C. Finocchiaro, M. Fugazzotto, C. Leonelli, M. José Lo, B. Megna, G. Barone, P. Mazzoleni, *Constr. Build. Mater.* **2020**, *259*, 120391.

[37] G. Barone, C. Finocchiaro, I. Lancellotti, C. Leonelli, P. Mazzoleni, C. Sgarlata, A. Stroscio, *Waste Biomass Valoriz.* **2021**, *12*(2), 1075. https://doi.org/10.1007/s12649-020-01004-6

[38] E. Murad, *Am. Mineral.* **1997**, *82*, 203.

[39] C. M. Belfiore, M. F. La Russa, P. Mazzoleni, A. Pezzino, M. Viccaro, *Environ Earth Sci* **2010**, *61*, 995.

[40] Y.-M. Liew, C. Y. Heah, M. M. Al Bakri, H. Kamarudin, *Prog. Mater. Sci.* **2016**, *83*, 595.

[41] C. Finocchiaro, G. Barone, P. Mazzoleni, C. Leonelli, A. Gharzouni, S. Rossignol, *Constr. Build. Mater.* **2020**, *262*, 120095.

[42] G. Barone, M. C. Caggiani, A. Coccato, C. Finocchiaro, M. Fugazzotto, G. Lanzafame, R. Occhipinti, A. Stroscio, P. Mazzoleni, *IOP Conf. Ser.: Mater. Sci. Eng.* **2020**, *777*(1), 012001.

[43] C. Finocchiaro, G. Barone, P. Mazzoleni, C. Sgarlata, I. Lancellotti, C. Leonelli, M. Romagnoli, *J. Mater. Sci.* **2021**, *56*, 513.

[44] B. Lafuente, R. T. Downs, H. Yang, N. Stone, in *Highlights in Mineralogical Crystallography*, (Eds: T. Armbruster, R. M. Danisi), De Gruyter, Berlin **2015**.

[45] B. Minčeva-Šukarova, A. İssi, A. Raškovska, O. Grupče, V. Tanevska, M. Yaygıngöl, A. Karab, P. Colomban, *J. Raman Spectrosc.* **2012**, *43*, 792.

[46] K. E. Kuebler, B. L. Jolliff, A. Wang, L. A. Haskin, *Geochim. Cosmochim. Ac.* **2006**, *70*(24), 6201.

[47] F. Froment, A. Tournié, P. Colomban, *J. Raman Spectrosc.* **2008**, *39*, 560.

[48] I. F. S. dos Santos, I. Hutchinson, R. Ingley, H. G. M. Edwards, D. L. A. de Faria, *Vib. Spectrosc.* **2016**, *87*, 20.

[49] V. Tanevska, P. Colomban, B. Minčeva-Šukarova, O. Grupče, *J. Raman Spectrosc.* **2009**, *40*, 1240.

[50] A. Zoppi, C. Lofrumento, E. M. Castellucci, P. Sciau, *J. Raman Spectrosc.* **2008**, *39*(1), 40.

[51] Y. Leon, C. Lofrumento, A. Zoppi, R. Carles, E. M. Castellucci, P. Sciau, *J. Raman Spectrosc.* **2010**, *41*(11), 1550.

[52] C. P. Marshall, W. J. B. Dufresne, C. J. Rufledt, *J. Raman Spectrosc.* **2020**, *51*, 1522.

[53] V. D'Ippolito, G. B. Andreozzi, D. Bersani, P. P. Lottici, *J. Raman Spectrosc.* **2015**, *46*, 1255.

[54] P. Colomban, *Appl. Phys. A: Mater. Sci. Process.* **2004**, *79*, 167.

[55] M. Arnoult, M. Perronnet, A. Autef, S. Rossignol, *J. Non-Cryst. Solids* **2018**, *495*, 59.

[56] G. E. Walrafen, *J. Chem. Phys.* **1975**, *62*, 297.

[57] R. J. H. Clark, Q. Wang, A. Correia, *J. Archaeol. Sci.* **2007**, *34*, 1787.

[58] P. Vargas Jentzsch, B. Kampe, V. Ciobota, *Spectrochim. Acta A-M* **2013**, *115*, 697.

[59] V. Košařová, D. Hradil, I. Němec, P. Bezdička, V. Kanický, *J. Raman Spectrosc.* **2013**, *44*, 1570.

[60] J. T. Kloprogge, *Developments in Clay Science* **2017**, *8*, 150.

[61] G. Renaudin, J. Russias, F. Leroux, C. Cau-dit-Coumes, F. Frizon, *J. Solid State Chem.* **2009**, *182*, 3320.

SUPPORTING INFORMATION

Additional supporting information may be found online in the Supporting Information section at the end of this article.